Role of Three-Dimensional Instabilities in Compliant Wall Boundary-Layer Transition

Ronald D. Joslin,* Philip J. Morris,† and Peter W. Carpenter‡
Pennsylvania State University, University Park, Pennsylvania 16802

The use of passive devices to obtain drag and noise reductions or transition delays in boundary layers is highly desirable. One such device that shows promise for hydrodynamic applications is the compliant coating. In the present study, a mechanical model is chosen to represent the compliant wall. In previous two-dimensional studies, coatings were found that provided significant transition delays. The present study allows for three-dimensional waves. These instabilities are found to dominate transition over compliant walls. However, transition delays are still obtained, compared with transition predictions for rigid walls. The angles of wave propagation and obliquity are determined as a function of Reynolds and frequency. The propagation or group velocity direction is found to be nearly axial. Calculations at fixed Reynolds numbers are also presented. These results indicate that the dominant mode for the coatings considered occurs for an oblique angle of approximately 40–60 deg. Other modes of instability that arise as a result of the compliance are discussed.

I. Introduction

THE use of compliant, or flexible, coatings for transition delays in boundary layers was stimulated by Kramer[1-5] in the late 1950s. Subsequent experiments failed to substantiate Kramer's results. However, a number of theoretical studies laid the foundation for all future studies with compliant walls. Among these are Benjamin,[6-8] Landahl,[9] and Gyorgyfalvy.[10] Benjamin and Landahl separated the modes of instability over a flexible surface into three classes: A, B, and C. Examples of these are the Tollmien-Schlichting instability (TSI), which is a class A instability, and traveling-wave flutter (TWF), which is a class B instability. The class C instability, which includes static divergence, takes the form of a Kelvin-Helmholtz instability and may be represented as a function of the surface properties only. Unlike conventional class C instabilities, static divergence is an absolute instability that when present destroys any transition delay potential that the surface may have otherwise had. Class A disturbances are generally destabilized by damping whereas class B disturbances are stabilized. Thus, attempts to stabilize class A instabilities have usually led to a destabilization of the class B instabilities.

Recent experiments by Daniel et al.,[11] Willis,[12] and Gaster[13] and theoretical investigations have been performed to develop an improved understanding of the instabilities arising from the fluid/solid interaction. These stem from the arguments made by Carpenter and Garrad.[14,15] They explain the deficiencies in the early experiments. Further, they argue that Kramer's coatings could lead to substantial delays in transition. Many other theoretical studies have been carried out in recent years, most of which have considered isotropic compliant-wall models similar to Refs. 14 and 15 or one- and two-layer isotropic coatings. By and large, these recent studies have confirmed that the use of wall compliance can confer considerable benefits in terms of reduction in instability growth rates and transition delay. Recent reviews of compliant-wall boundary-layer research have been given by Carpenter[16] and Riley et al.[17]

Many previous studies have focused on two-dimensional instabilities over compliant walls. However, the effective wall compliance decreases as the mainstream flow speed drops. Thus, as pointed out by Yeo,[18] since obliquely propagating waves have a reduced effective mainstream speed as compared with two-dimensional waves, oblique TSI would experience reduced effective wall compliance. Consequently, the stabilizing effects of wall compliance on oblique TSI would be reduced as compared with their two-dimensional counterparts. This may well result in oblique TSI growing more rapidly over a compliant wall than the corresponding two-dimensional waves. In fact, this is in evidence in the results presented by Yeo[18] and Carpenter and Morris[19,20] in a preliminary study. In the present paper, we present the results of a detailed investigation of the effect of wall compliance on both two- and three-dimensional disturbances in the form of traveling waves. Comparisons are made of the growth rates of these disturbances over isotropic and nonisotropic compliant walls with the rigid wall case. We choose, as representative examples, particular isotropic and nonisotropic coatings that show significant transition delays in the two-dimensional case. The properties of the coatings were given by Carpenter and Morris.[19-21] The optimization procedure involves making the wall instabilities, TWF, and static divergence marginally stable and then reducing the Tollmien-Schlichting instability to meet some desired goal. This would be either a local reduction in growth rate or a reduction in the overall amplitude growth of the wave. We use the e^n method of Smith and Gamberoni[22] to make transition predictions for two- and three-dimensional traveling waves.

In the present analysis the compliant wall is represented by a mechanical model. The model is based on a concept by Grosskreutz[23,24] that he used in his study of drag reduction in turbulent boundary layers. He proposed that such a surface would lead to a negative production of Reynolds stress near the wall. This was achieved by linking the streamwise and normal motions of the surface. Although his experimental

Presented as Paper 90-0115 at the AIAA 28th Aerospace Sciences Meeting, Reno, NV, Jan. 8-11, 1990; received March 23, 1990; revision received Dec. 4, 1990; accepted for publication Dec. 6, 1990.

*Graduate Student, Department of Aerospace Engineering; currently Research Scientist, NASA Langley Research Center, Hampton, VA. Member AIAA.

†Professor, Department of Aerospace Engineering. Senior Member AIAA.

‡Visiting Professor; permanently Professor of Mechanical Engineering. School of Engineering, University of Warwick, England, UK.

results were disappointing, such a concept is appealing particularly for delaying transition in laminar boundary layers. The model has been investigated previously by Carpenter and Morris[21] and Joslin and Morris[25] for two-dimensional transitional boundary layers. Their results indicate that an appropriate choice of wall properties leads to a significant reduction in the flow instability growth rates without the introduction of static divergence or the occurrence of significant growths of other wall instabilities. Further, substantial delays of transition are predicted as compared to the rigid wall calculations.

In the present paper, we extend the study to three-dimensional instabilities over a compliant wall. The problem takes the form of an eigenvalue problem where the eigenvalue appears nonlinearly and is of the highest order in the boundary conditions. The problem is formulated in the next section. A number of methods of solution are available that have been implemented by the authors. In this paper a local shooting method is used. The method is outlined in the third section. The results and conclusions follow in the fourth and fifth sections, respectively.

II. Theoretical Model

In this analysis we assume that the laminar boundary-layer flow is parallel and is represented by the Blasius profile $U_o(y)$. A disturbance is introduced into the boundary layer and grows or becomes damped as it propagates with the flow. The disturbance takes the form of a traveling wave. A normal mode representation is given as

$$v(x,y,z,t) = \hat{v}(y)E + \text{c.c.} \tag{1}$$

where $\hat{v}$ is a complex eigenfunction; the pressure and vorticity fluctuations, etc., are represented in a similar manner. In the general case

$$E = \exp[i(\alpha x + \beta z - \omega t)] \tag{2}$$

where α and β are complex wave numbers and ω is a complex frequency. For three-dimensional temporal instabilities, α and β are both real, and ω is the complex eigenvalue. For the more realistic case of spatially growing waves, one can follow Nayfeh[26] and define a wave number vector (α_r,β_r) with a wave angle of $\phi_w = \tan^{-1}(\beta_r/\alpha_r)$ and a growth rate vector (α_i,β_i) with direction $\phi_g = \tan^{-1}(\beta_i/\alpha_i)$. In general, ϕ_w and ϕ_g are not equal. However, Nayfeh[26] and Cebeci and Stewartson[27] use the saddle point method to show that far from a disturbance source the fluctuation is dominated by wave components for which

$$\frac{d\alpha}{d\beta} + \frac{z}{x} = 0 \tag{3}$$

For real values of z/x, the Cauchy-Riemann equations require that

$$\frac{\partial\alpha_r}{\partial\beta_r} = \frac{-z}{x}, \qquad \frac{\partial\alpha_i}{\partial\beta_r} = 0 \tag{4}$$

Thus, the group velocity angle that defines the direction of energy propagation is given by

$$\bar{\phi} = -\tan^{-1}\left(\frac{\partial\alpha_r}{\partial\beta_r}\right) \tag{5}$$

The axial growth rate of the fixed frequency wave is given by

$$\Gamma = -(\alpha_i + \beta_i \tan\bar{\phi}) \tag{6}$$

However, Eq. (4) does not remove all arbitrariness from the problem. In addition, we may require that the growth rate in Eq. (6) be maximized. It is shown in the following that $\tan\bar{\phi}$ is small, particularly when $|\alpha_i|$ is large. Thus, a reasonable estimate of the growth rate is obtained by setting

$$\Gamma \approx -\alpha_i, \qquad \text{with} \qquad \frac{\partial\alpha_i}{\partial\beta_r} = 0 \tag{7}$$

The growth rate given by Eq. (7) is used in the e^n calculations. However, as a simpler preliminary study of local three-dimensional effects, we also consider the representation

$$E = \exp[i(\gamma\cos\phi x + \gamma\sin\phi z - \omega t)] \tag{8}$$

This assumes that $\phi_w = \phi_g$ ($=\phi$, say) that, as noted above, is not true in general. The results of calculations using Eq. (8) are related to the local growth of a disturbance that has an imposed obliquity. This could be introduced by a wavemaker or heating strips as used by Corke and Mangano.[28] The advantage of this formulation is that it is simpler and does provide a qualitative picture of the relative growth of the two- and three-dimensional disturbances for various wall properties. The subsequent analysis uses the representation of Eq. (8), although calculations have been performed using both this representation and that of Eq. (2).

The variables are nondimensionalized with respect to the boundary-layer displacement thickness δ^* (or the boundary-layer thickness δ), the freestream velocity U_∞, and density ρ. The Reynolds number is given by $R_{\delta^*} = U_\infty\delta^*/\nu$, and R_x is the Reynolds number based on x. Three-dimensional disturbances can be shown to satisfy the Orr-Sommerfeld equation and Squire's equation in terms of the normal velocity ($\hat{v}$) and vorticity ($\hat{\Omega}$), respectively. These equations are

$$\hat{v}^{iv}(y) + a_1(y)\hat{v}''(y) + a_2(y)\hat{v}(y) = 0 \tag{9}$$

where

$$a_1(y) = -2\gamma^2 - iR_\delta[\gamma\cos\phi U_o(y) - \omega]$$

$$a_2(y) = \gamma^4 + i\gamma^2 R_\delta[\gamma\cos\phi U_o(y) - \omega] + iR_\delta\gamma\cos\phi U_o''(y)$$

and

$$\hat{\Omega}''(y) + a_3(y)\hat{\Omega}(y) + a_4(y)\hat{v}(y) = 0 \tag{10}$$

where

$$a_3(y) = -\gamma^2 - iR_\delta[\gamma\cos\phi U_o(y) - \omega]$$

$$a_4(y) = -iR_\delta\gamma\sin\phi U_o'(y)$$

We require that the velocity fluctuations vanish far from the wall. So the far-field boundary conditions may be written

$$\hat{v}(y), \quad \hat{v}'(y), \quad \hat{\Omega}(y) \to 0 \quad \text{as} \quad y \to \infty \tag{11}$$

The remaining three boundary conditions are derived from the equations governing the motion of the compliant wall.

The theoretical model for the wall consists of a thin, elastic plate supported by hinged and sprung rigid members inclined to the horizontal at an angle θ, when in equilibrium. The model is illustrated in Fig. 1. The surface is permitted to move in both the horizontal and vertical directions. The motion of the plate is treated such that each element of the plate can oscillate in a pendulum-like motion about its rigid member. The distance between each member is assumed to be much smaller than a characteristic wavelength of the flow instability. This mechanical model may be regarded as an approximate model for a flexible plate supported by fiber-composite sheets or a thin plate supported by ribs that extend spanwise. Thus, it becomes comparatively stiff in the spanwise direction.

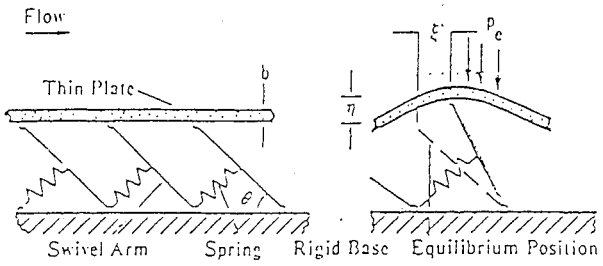

Fig. 1 Schematic of theoretical model of a nonisotropic compliant wall.

For small displacements of an element out of equilibrium, the surface moves in a direction perpendicular to the rigid swivel arm. The equation of motion for the element is obtained such that the total force acting on the surface by the fluid fluctuations is balanced by the forces due to the wall properties. Let (x,y,z) be the streamwise, normal, and spanwise independent coordinates; let (ξ,η,ζ) be the streamwise, normal, and spanwise surface displacements; $\delta\theta$ is the angular displacement of the element relative to the equilibrium position; ℓ is the swivel-arm length; ρ_m and b are the plate density and thickness; B_x, B_{xz}, and B_z are the flexural rigidities of the plate in the streamwise, transverse, and spanwise directions; E_x and E_z are the moduli of elasticity of the plate in the streamwise and spanwise directions; K_E is the effective spring stiffness; and p, σ, and τ are the pressure, viscous normal stress, and viscous streamwise shear stress fluctuations in the fluid acting on the wall. Then, in the streamwise direction the resulting equation is given as

$$\rho_m b\frac{\partial^2\eta}{\partial t^2} + \left(B_x\frac{\partial^4\eta}{\partial x^4} + 2B_{xz}\frac{\partial^4\eta}{\partial x^2\partial z^2} + B_z\frac{\partial^4\eta}{\partial z^4}\right)\cos^2\theta + K_E\eta - E_x b\frac{\partial^2\xi}{\partial x^2}\sin\theta\cos\theta = -p\cos^2\theta + \sigma\cos^2\theta + \tau\sin\theta\cos\theta \tag{12}$$

The terms of the left-hand side of Eq. (12) refer to mechanical forces, and the terms on the right-hand side refer to fluid motion forces due to viscous stress and pressure fluctuations. For $\theta = 0$ deg the wall becomes isotropic and reduces to the theoretical model studied by Carpenter and Garrad.[14,15] Otherwise the wall is referred to as nonisotropic, and the rib angle is determined by θ. For $E_x = E_z$ the plate is described as isotropic, and for $E_x \neq E_z$ the plate is orthotropic.

The effective spring stiffness incorporates the body forces such that

$$K_E = K - g(\rho - \rho_g)\cos\theta \tag{13}$$

where K is the spring stiffness, g is the acceleration due to gravity, and ρ_g is the substrate density. In this investigation, we will only consider the case where the fluid and substrate have the same density ($\rho = \rho_g$), so $K_E = K$.

The flexural rigidities can be found from the relations

$$B_x = \frac{E_x b^3}{12(1-\nu_x\nu_z)}, \qquad B_z = \frac{E_z b^3}{12(1-\nu_x\nu_z)} \tag{14}$$

where ν_x and ν_z are the corresponding Poisson ratios. For elastomeric materials, such as would be used for manufacturing a practical compliant wall, the Poisson ratio is usually very close to 0.5. It is therefore assumed $\nu_x = \nu_z = 0.5$. A reasonable model for B_{xz} is given by

$$B_{xz} = \sqrt{B_x B_z} \tag{15}$$

As well as Eq. (7), we enforce continuity of motion between the fluid and wall. The linearized streamwise, normal, and spanwise continuity equations are given by

$$\frac{\partial\xi}{\partial t} = u + \eta\frac{dU_o}{dy} \tag{16}$$

$$\frac{\partial\eta}{\partial t} = v \tag{17}$$

$$\frac{\partial\zeta}{\partial t} = w \tag{18}$$

It is assumed that the swivel-arm, or rib, for a given element's orientation is such that the streamwise and normal wall motion will have a much greater freedom of motion than the spanwise. This suggests that $\zeta << \eta, \xi$ so we let $\zeta = 0$. From Eq. (18) we then find that the spanwise fluctuation at the wall is zero, or $w = 0$. This is a reasonable approximation and is in agreement with the characteristics of the Grosskreutz coating under consideration. An alternative wall might consist of stiffening fibers embedded in a softer matrix. In this case, this simplification may not hold. It has been found in other calculations that this freedom in the spanwise direction leads to slightly larger instability growth rates as compared with the model considered in the present paper.

The equations of motion for the surface are coupled by a relationship between the streamwise and normal displacements (ξ,η) and the angular displacement $(\delta\theta)$ such that

$$\xi = \ell\delta\theta\sin\theta, \qquad \eta = \ell\delta\theta\cos\theta \tag{19}$$

The displacement of the surface may be represented in the same normal mode fashion as the velocity and vorticity. If these relationships are substituted into the equation of motion for the wall, its nondimensional form is given by

$$[-C_M\omega^2 + (C_{Bx}\cos^4\phi + 2C_{Bxz}\sin^2\phi\cos^2\phi + C_{Bz}\sin^4\phi)\gamma^4\cos^2\theta + C_K + C_T\gamma^2\sin^2\theta\cos^2\phi]\hat{\eta} = -\hat{p}\cos^2\theta + \hat{\sigma}\cos^2\theta + \hat{\tau}\sin\theta\cos\theta \tag{20}$$

where

$$C_{Bx} = \frac{B_x}{\rho U_\infty\delta^{*3}}, \quad C_{Bxz} = \frac{B_{xz}}{\rho U_\infty\delta^{*3}}, \quad C_{Bz} = \frac{B_z}{\rho U_\infty\delta^{*3}}$$
$$C_m = \frac{\rho_m b}{\rho\delta^*}, \quad C_K = \frac{K\delta^*}{\rho U_\infty^2}, \quad C_T = \frac{E_x b}{\rho U_\infty^2\delta^*} \tag{21}$$

Similarly, substitution of solutions of the form of Eq. (1) into the streamwise and normal continuity equations, Eqs. (16) and (17), gives

$$[U_o'(0)\cos\theta + i\omega\sin\theta]\hat{\eta} = -\hat{u}(0)\cos\theta \tag{22}$$

$$\hat{\eta}\omega = i\hat{v}(0) \tag{23}$$

The viscous stresses and pressure fluctuations at the wall are obtained from the fluid equations of motion. This leads to three boundary conditions for the normal velocity and normal vorticity fluctuations given by

$$\gamma^5[(C_{Bx}\cos^4\phi + 2C_{Bxz}\cos^2\phi\sin^2\phi + C_{Bz}\sin^4\phi)\cos^2\theta\hat{v}'(0)] + \gamma^3[C_T\sin^2\theta\cos^2\phi\hat{v}'(0)] + \gamma^2\{[2\omega\sin\theta - 3iU_o'(0)\cos\theta]\cos\theta\cos\phi\frac{1}{R}\hat{v}'(0) - [U_o'(0)\cos\theta + i\omega\sin\theta]\sin\theta\sin\phi\cos\phi\frac{1}{R}[\cos\phi\Omega'(0)$$

$$+ \sin\phi\hat{v}''(0)]\} + \gamma\{(C_K - \omega^2 C_M)\hat{v}'(0) + [U_o'(0)\cos\theta$$

$$+ i\omega\sin\theta]\sin\theta\frac{1}{R}\hat{v}''(0)\} + \{-i\omega^2\cos\theta\sin\theta\cos\phi\hat{v}'(0)$$

$$+ i[U_o'(0)\cos\theta + i\omega\sin\theta]\cos\theta\cos\phi\frac{1}{R}\hat{v}'''(0)\} = 0 \quad (24)$$

$$\gamma\cos\phi[U_o'(0)\cos\theta + i\omega\sin\theta]\hat{v}(0) + \omega\cos\theta\hat{v}'(0) = 0 \quad (25)$$

$$\hat{\Omega}(0) + \tan\phi\hat{v}'(0) = 0 \quad (26)$$

To simulate the rigid wall case, we let $C_M \to \infty$. In this way the above boundary conditions reduce to that for the rigid plate.

III. Numerical Method

In this section we consider the numerical approach used to solve the system of equations and boundary conditions representing linear transition over a compliant wall. The approach is a local-shooting method. Although spectral methods have distinct advantages and have been employed by the authors and a number of other investigators, the local method proves to be much faster computationally and more suitable for the present study.

The Orr-Sommerfeld and Squire's equations, Eqs. (9) and (10), respectively, may be arranged into the following system of first-order ordinary differential equations:

$$D\begin{Bmatrix}\hat{v}'''\\ \hat{v}''\\ \hat{v}'\\ \hat{v}\\ \hat{\Omega}'\\ \hat{\Omega}\end{Bmatrix} = \begin{pmatrix}0 & -a_1 & 0 & -a_2 & 0 & 0\\ 1 & 0 & 0 & 0 & 0 & 0\\ 0 & 1 & 0 & 0 & 0 & 0\\ 0 & 0 & 1 & 0 & 0 & 0\\ 0 & 0 & 0 & -a_4 & 0 & -a_3\\ 0 & 0 & 0 & 0 & 0 & 1\end{pmatrix}\begin{Bmatrix}\hat{v}'''\\ \hat{v}''\\ \hat{v}'\\ \hat{v}\\ \hat{\Omega}'\\ \hat{\Omega}\end{Bmatrix} \quad (27)$$

This is the appropriate form for the Runge-Kutta integration routine. In general, the form of the boundary conditions for the above system given by Eqs. (24–26) is

$$\bar{a}_1\hat{v}'(0) + \bar{a}_2\hat{v}''(0) + \bar{a}_3\hat{v}'''(0) + \bar{a}_4\hat{\Omega}'(0) = 0 \quad (28)$$

$$\bar{a}_5\hat{v}(0) + \bar{a}_6\hat{v}'(0) = 0 \quad (29)$$

$$\hat{\Omega}(0) + \bar{a}_7\hat{v}'(0) = 0 \quad (30)$$

At the wall the general solution for the sixth-order system may be written

$$\begin{Bmatrix}\hat{v}'''\\ \hat{v}''\\ \hat{v}'\\ \hat{v}\\ \hat{\Omega}'\\ \hat{\Omega}\end{Bmatrix} = A_1\begin{Bmatrix}1\\0\\0\\0\\0\\0\end{Bmatrix} + A_2\begin{Bmatrix}0\\1\\0\\0\\0\\0\end{Bmatrix} + \cdots + A_6\begin{Bmatrix}0\\0\\0\\0\\0\\1\end{Bmatrix} \quad (31)$$

Using the boundary conditions, Eqs. (28–30), three of the unknown coefficients may be eliminated giving three linearly independent solutions in the form

$$\begin{Bmatrix}\hat{v}'''\\ \hat{v}''\\ \hat{v}'\\ \hat{v}\\ \hat{\Omega}'\\ \hat{\Omega}\end{Bmatrix} = A\begin{Bmatrix}0\\1\\\hat{v}_1'\\\hat{v}_1\\0\\\hat{\Omega}_1\end{Bmatrix} + B\begin{Bmatrix}1\\0\\\hat{v}_2'\\\hat{v}_2\\0\\\hat{\Omega}_2\end{Bmatrix} + C\begin{Bmatrix}0\\0\\\hat{v}_3'\\\hat{v}_3\\1\\\hat{\Omega}_3\end{Bmatrix} \quad (32)$$

where

$$\hat{v}_1' = -\bar{a}_2/\bar{a}_1, \quad \hat{v}_2' = -\bar{a}_3/\bar{a}_1, \quad \hat{v}_3' = -\bar{a}_4/\bar{a}_1$$

$$\hat{v}_1 = -\bar{a}_6/\bar{a}_5\hat{v}_1', \quad \hat{v}_2 = -\bar{a}_6/\bar{a}_5\hat{v}_2', \quad \hat{v}_3 = -\bar{a}_6/\bar{a}_5\hat{v}_3'$$

$$\hat{\Omega}_1 = -\bar{a}_7\hat{v}_1', \quad \hat{\Omega}_2 = -\bar{a}_7\hat{v}_2', \quad \hat{\Omega}_3 = -\bar{a}_7\hat{v}_3'$$

Beginning with these vectors at the wall, we integrate across the boundary layer using a 5th-order Runge-Kutta scheme. Linear independence is maintained using Gramm-Schmidt orthonormalization. The orthonormalization is implemented whenever a vector's magnitude exceeds 10^3. A final orthonormalization is applied at the outer edge of the boundary layer.

Outside the boundary layer, the solutions satisfying the boundary conditions at infinity, Eq. (11), may be written

$$\hat{v} = B_1 e^{-\gamma y} + B_2 e^{-\bar{\gamma} y} \quad (33)$$

$$\hat{\Omega} = B_3 e^{-\bar{\gamma} y} \quad (34)$$

where

$$\bar{\gamma} = \sqrt{\gamma^2 + iR_\delta(\gamma\cos\phi - \omega)}, \qquad Re\{\bar{\gamma}\} > 0$$

The numerical solutions are matched with the three linearly independent solution vectors formed from Eqs. (33) and (34) at the edge of the boundary layer. This gives a 6 × 6 homogeneous system of equations for the unknown coefficients, A, B, C, B_1, B_2, and B_3. For a nontrivial solution, the determinant of the system must be zero. At a given Reynolds number and frequency, the wave number is altered until this condition is met.

The focus of this paper is on the evolution of the Tollmien-Schlichting waves as they grow and decay. Traveling-wave flutter, which is a class B instability, is marginally stable for the selected wall properties. However, this instability is also monitored to determine if it remains marginally stable in the three-dimensional case. An asymptotic theory due to Carpenter and Gajjar[29] may be used for this purpose.

IV. Results

In all of the cases considered, the freestream velocity U_∞ is 20 m/s, the density ρ is 1000 kg/m^3, and the kinematic viscosity ν is 1×10^{-6} m^2/s. The coatings that will be used in evaluating the effect of compliance on three-dimensional instabilities consist of an isotropic and a nonisotropic wall.

The wall properties have been optimized using the procedure described by Carpenter and Morris.[19] The procedure consists of requiring that the TWF and static divergence are marginally stable based on an asymptotic theory. A remaining free parameter that depends on the wall properties is then varied to obtain the minimum Tollmien-Schlichting growth rate at a given Reynolds number. For the majority of the present calculations, this Reynolds number is $R_{\delta^*} = 2240$. However, some calculations have been performed for walls with the Tollmien-Schlichting growth rates minimized at $R_{\delta^*} = 5000$. The wall properties are given in Table 1. For convenience, the different cases are referred to as walls 1, 2, and 3. The results of the two-dimensional instability calculations over these coatings and the rigid wall are used for a comparison with the present three-dimensional results. In the present paper, we also consider the development of three-dimensional instability waves over walls with both isotropic and orthotropic plates. The properties for the isotropic plate are direction independent and $E_x = E_z = E_{xz}$. The orthotropic plate has $E_z = 0$ and so is very compliant in the spanwise direction. This gives four coating combinations of interest. These cases will be referred to as the isotropic wall/isotropic

Table 1 Optimal wall properties, R_{min} denotes the value of R_{δ^*} at which the Tollmien-Schlichting growth rates are minimized

	θ, deg	R_{min}	b, mm	E_x, MN/m^2	K_E, GN/m^3
Wall 1	0	2240	0.735	1.385	0.354
Wall 2	60	2240	0.111	0.509	0.059
Wall 3	60	5000	0.334	0.507	0.0197

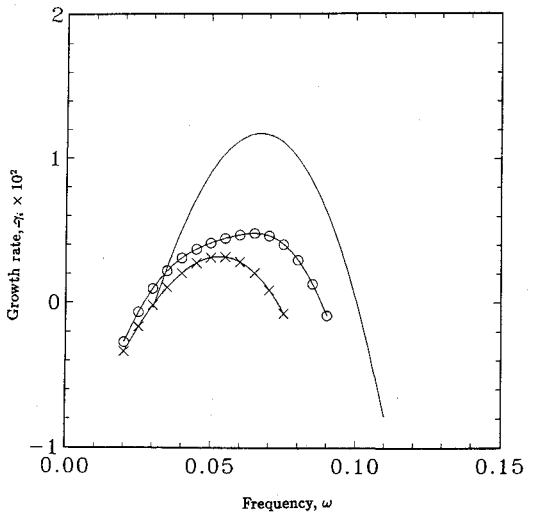

Fig. 2 Two-dimensional growth rates as a function of frequency; rigid wall, ——; compliant walls, θ = 0 deg, –○–; θ = 60 deg, – × –; R_{δ^*} = 2240.

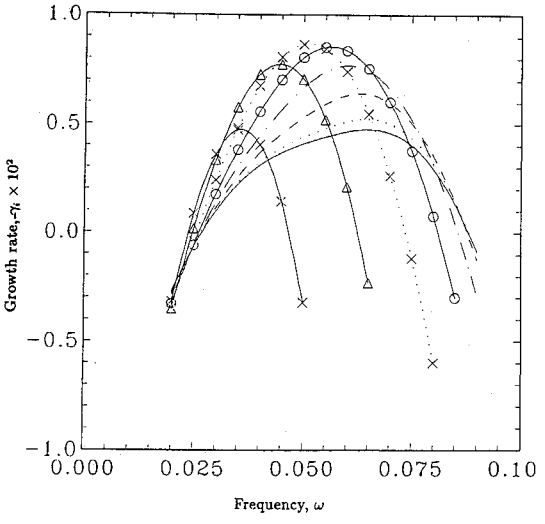

Fig. 3 Growth rates as a function of frequency for a θ = 0 deg wall/isotropic plate, R_{δ^*} = 2240; oblique wave angles ϕ_w; 0 deg, ——; 10 deg, ·····; 20 deg, – – –; 30 deg, – · –; 40 deg, –○–; 50 deg, ··· × ···; 60 deg, –△–; 70 deg, – × –.

plate, isotropic wall/orthotropic plate, nonisotropic wall/isotropic plate, and nonisotropic wall/orthotropic plate.

As a first case, we consider the three-dimensional instabilities for a fixed displacement thickness Reynolds number of 2240. The local formulation given by Eq. (8) is used. Thus the growth rate in the direction normal to the wave front is given by $-\gamma_i$. Figure 2 shows the growth rates of the two-dimensional waves for various frequencies for the compliant walls 1 and 2 and a rigid wall. For the nonisotropic wall with θ = 60 deg, the maximum growth rate is about 25% of that for the rigid wall. The width of the unstable region is $\omega - R_{\delta^*}$ space is also reduced considerably for the compliant walls as compared to the rigid surface. Figures 3 and 4 show the growth rates as a function of frequency for various wave angles ϕ propagating over the same two compliant walls. For both

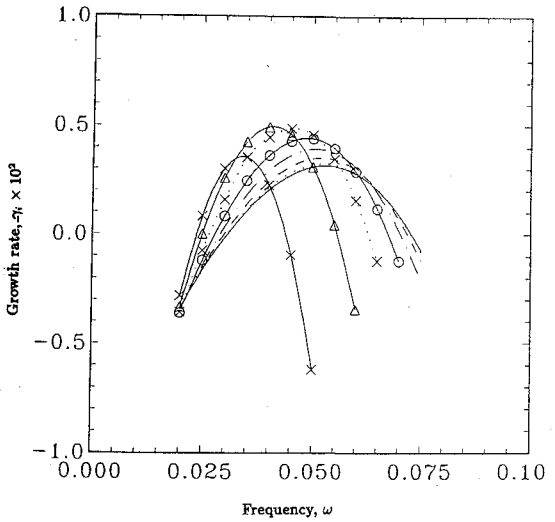

Fig. 4 Growth rates as a function of frequency for a θ = 60 deg wall/isotropic plate; R_{δ^*} = 2240 (for legend see Fig. 3).

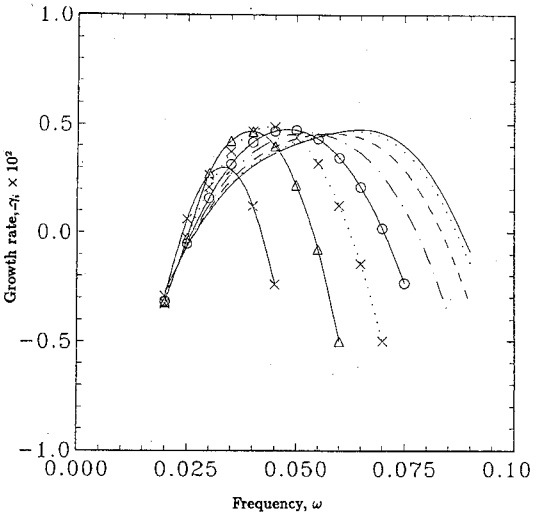

Fig. 5 Growth rates as a function of frequency for a θ = 0 deg wall/orthotropic plate; R_{δ^*} = 2240 (for legend see Fig. 3).

coatings, the maximum growth rates are found for three-dimensional waves with wave angles of 50–60 deg to the flow direction. In the isotropic case, an approximately 60% increase in growth rate over the two-dimensional case is found. For the nonisotropic wall, the dominance of the three-dimensional waves is considerably reduced but is still quite marked. The reduced sensitivity of the nonisotropic compliant wall to three-dimensional waves compared to the isotropic case can be attributed to the effects of irreversible energy exchange between the wall and the disturbance due to the work done by the fluctuating shear stress. Carpenter and Morris[19] showed that this energy exchange has a relatively destabilizing effect on the Tollmien-Schlichting waves that grows as θ increases. This deleterious effect is reduced for oblique waves owing to the reduced magnitude of the fluctuating shear stress in the direction normal to the wave fronts. This results in the relative improvement in terms of reductions in the three-dimensional growth rates and range of unstable frequencies for nonisotropic as compared to isotropic compliant walls.

The increased instability of the three-dimensional waves is caused by the reduced effective wall compliance for oblique waves. Accordingly, Yeo[18] and Carpenter[30] have suggested that increasing the compliance in the spanwise direction by using an orthotropic plate may well reduce the growth rates of the oblique waves. It is apparent from Fig. 5 that this

strategy is successful for the isotropic wall/orthotropic plate case. The three-dimensional waves are now no longer the most unstable. However, the orthotropic plate used was $E_z = 0$ that is the extreme case and may not be practical. For the nonisotropic wall/orthotropic plate case illustrated in Fig. 6, there is little change from the isotropic plate case shown in Fig. 4. The reason for this is readily found from a consideration of the equation of motion for the wall given by Eq. (12). For the isotropic ($\theta = 0$ deg) case, all the wave number dependent stiffness resides in the bending-stiffness terms ($B_x\partial^4\eta/\partial x^4$, etc.). For nonisotropic compliant walls with nonzero θ, on the other hand, much of the wave number dependent stiffness is also contributed by the induced-tension term ($E_x\partial^2\xi/\partial x^2 \sin\theta \cos\theta$). For $\theta = 60$ deg, this second contribution to the stiffness is relatively large and is, of course, unaffected by the use of an orthotropic plate.

To confirm these local calculations, e^n calculations have been performed. Figure 7 shows curves of maximum amplification for two-dimensional waves in the frequency range of interest for the compliant and rigid walls. These two-dimensional calculations agree with Carpenter and Morris.[19] Some controversy exists as to which value of n is the proper indication of transition. But if we choose a conservative value of $n = 7$, a delay of approximately 4–5 times the rigid wall transition Reynolds number may be realized. However, for higher values of n, the advantages of the wall compliance increase.

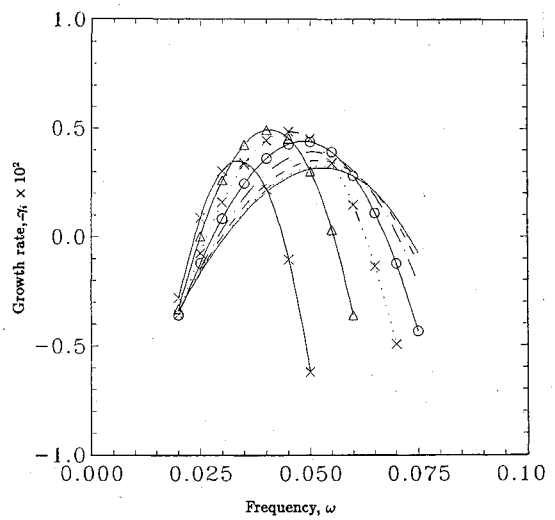

Fig. 6 Growth rates as a function of frequency for a $\theta = 60$ deg wall/orthotropic plate; $R_{\delta^*} = 2240$ (for legend see Fig. 3).

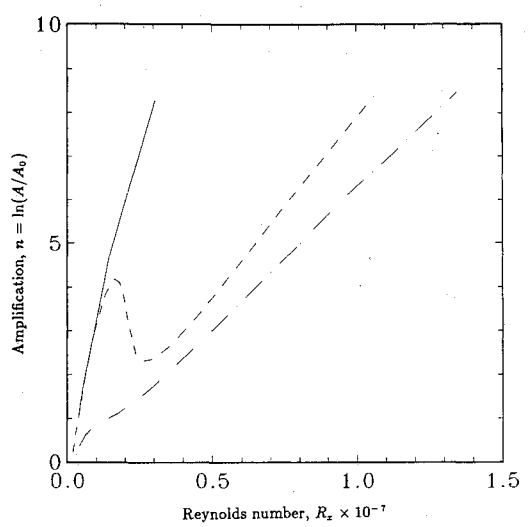

Fig. 7 Two-dimensional curves of maximum amplification; rigid wall, —; compliant walls, $\theta = 0$ deg, – – –; $\theta = 60$ deg, – · –.

As discussed in Sec. II, the extension of the e^n method to the case of three-dimensional disturbances has yet to be resolved satisfactorily, even for rigid surfaces. A complete calculation, appropriate for natural transition or forcing from a point source, would involve locating the "zarf" for a given frequency as defined by Cebeci and Stewartson.[27] A fixed frequency disturbance would then be followed in the direction of the group velocity or propagation angle given by Eq. (5). The total growth would be obtained by maximizing the axial growth given by Eq. (6). Such a calculation is computationally expensive. However, for the walls considered here the propagation angle is relatively small. For example, Fig. 8 shows the propagation for the isotropic wall 1 and frequency parameter $Fr = \omega/R_{\delta^*} = 30.22$ as a function of R_{δ^*}. Also shown are the wave angle $\phi_w = \tan^{-1}(\beta_r/\alpha_r)$ for maximum axial growth rate and the axial growth rate $-\alpha_i$. It can be seen that ϕ has a maximum of 0.14 at the lower branch and rapidly decreases with increasing R_{δ^*}. In the region of maximum axial growth, ϕ is less than 0.01. These calculations are for $\beta_i = 0$ but are similar for other values of β_i. Thus, in the present e^n calculations, a good estimate of the overall axial growth is given by

$$n = \ln(A/A_0) = -\int_{x_0}^{x} \alpha_i(x')\,dx' \tag{35a}$$

where

$$\frac{\partial\alpha_i}{\partial\beta_r} = 0, \qquad \beta_i = 0 \tag{35b}$$

The value of x_0 is obtained by starting the calculations on the two-dimensional neutral curve for a given frequency. The spanwise wave number is then varied to find its value for maximum axial growth rate. Finally, the Reynolds is reduced, keeping $\partial\alpha_i/\partial\beta_r = 0$ until the value of $\alpha_i = 0$. This is very close to the location of the zarf defined by Cebeci and Stewartson.[27]

Figure 9 shows e^n calculations for three-dimensional disturbances over the isotropic wall 1 based on Eq. (35). As might be expected from the local calculations presented earlier, the overall growth with the orthoptropic plate is less than that for the isotropic plate. The amplitude ratio factor for $Re_x = 0.25 \times 10^6$ is considerably less for the orthotropic plate. This is close to the Reynolds number at which the plate properties were optimized. Once again, choosing a conservative value of $n = 7$ to indicate transition, the three-dimensional

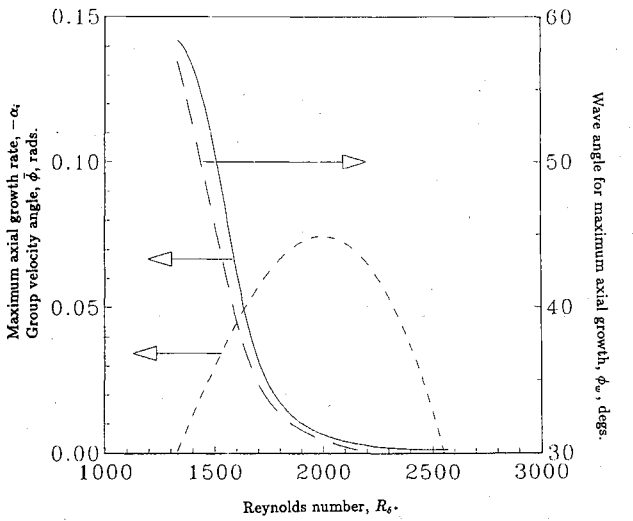

Fig. 8 Variation of wave properties with Reynolds number; compliant, $\theta = 0$ deg wall/isotropic plate, $Fr = 30.22$; axial growth rate $-\alpha_i$, – – –; wave angle for maximum axial growth ϕ_w, ——; group velocity angle ϕ, ——.

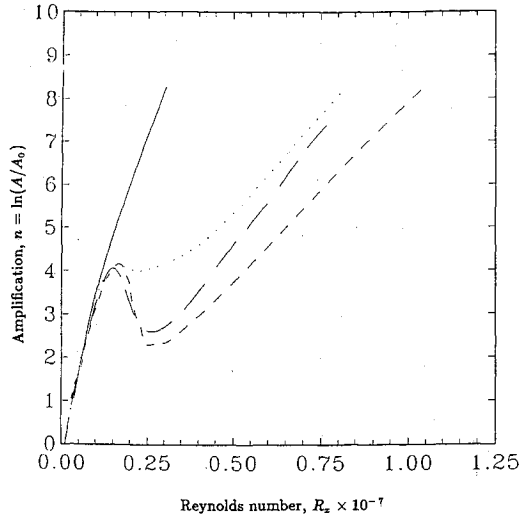

Fig. 9 Two- and three-dimensional curves of maximum amplification; two-dimensional rigid wall, —; compliant walls, two-dimensional θ = 0 deg, ---; three-dimensional θ = 0 deg orthotropic plate, ——; three-dimensional θ = 0 deg isotropic plate, ·····. R_{min} = 2240.

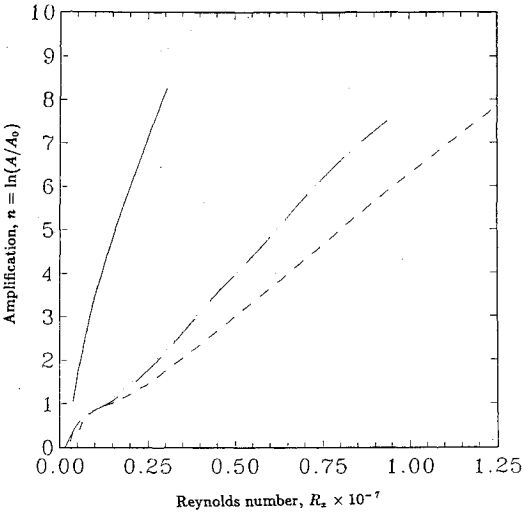

Fig. 10 Two- and three-dimensional curves of maximum amplification; two-dimensional rigid wall, ——; compliant walls, two-dimensional θ = 60 deg, ---; three-dimensional θ = 60 deg orthotropic plate, ——; three-dimensional θ = 60 deg isotropic plate, ·····. R_{min} = 2240.

calculations indicate a factor of three delay in transition compared to the rigid wall. The two-dimensional calculations, also shown in Fig. 9, indicate a factor of four transition delay.

Similar calculations are shown for the nonisotropic wall 2 in Fig. 10. As expected from the local calculations, Figs. 4 and 6, there is almost no difference between the isoptropic and orthotropic plate cases. The transition delay is predicted to be slightly greater for this wall than the isotropic wall shown in Fig. 9. However, the delay is less than that predicted for the two-dimensional disturbances.

Figure 11 shows the amplitude ratio factor for the nonisotropic wall 3. In this case, the wall properties were optimized at R_{δ^*} = 5000 (see Table 1). The initial growth is similar to the rigid wall case. This shows that the higher frequency instabilities are relatively unaffected by the change in wall properties. However, by optimizing the wall properties at a higher local Reynolds number, it can be seen that the amplitude ratio is maintained at a nearly constant level, below the critical value of 7, for a large axial distance. This trend was observed in the two-dimensional calculations and continues to be evident when three-dimensional disturbances are considered. It is clear that a surface that had properties that varied in the

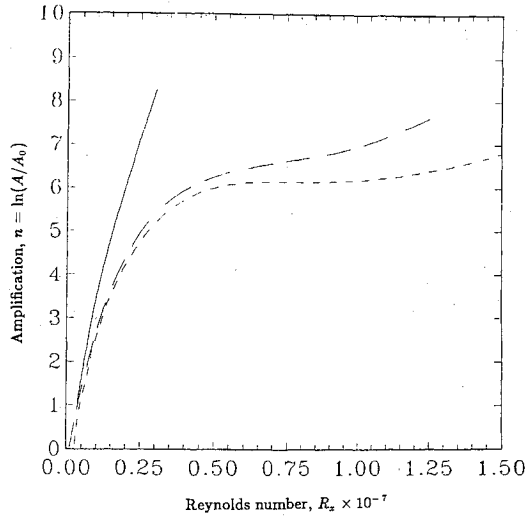

Fig. 11 Two- and three-dimensional curves of maximum amplification; rigid wall, ——; compliant walls, two-dimensional θ = 60 deg, ---; three-dimensional θ = 60 deg, isotropic plate, ——; R_{min} = 5000.

streamwise direction, perhaps by the use of short sections with different properties, could lead to additional increases in the predicted transition delay.

To this point we have neglected any consideration of TWF. In this we have assumed that this instability wave remains marginally stable and transition continues to be governed by the Tollmien-Schlichting instability growth. Carpenter and Gajjar[29] performed a temporal analysis based on an asymptotic theory to examine the instability of oblique TWF modes. For the walls considered here, it is shown that TWF remains marginally stable with a very small region of weakly unstable wave numbers. The oblique waves are found to be more stable than the two-dimensional ones. As was stated in the modal classification, mechanisms that destabilize class A waves tend to stabilize class B waves. Calculations with the orthotropic plate show a slight destabilizing effect over the isotropic plate case. Nevertheless, the effect is relatively small, and the results suggest that there would be no problem with TWF if orthotropic plates were to be used.

V. Conclusions

The present paper has considered the growth of three-dimensional disturbances over various models of compliant walls. For all the coatings considered the largest growth rates were obtained for three-dimensional Tollmien-Schlichting waves. Two methods of examining the effects of three-dimensionality were considered. In the first, the local growth rates in the direction normal to the wave fronts was examined. This simple calculation allows the different compliant walls and their effect on three-dimensional disturbances to be examined. However, for the e^n calculations the overall axial growth was obtained at a given frequency by following the wave with the maximum axial growth rate in the axial direction. This is justified since the group velocity angle is very small, except near the lower branch where the growth rates are themselves small.

The calculations showed significant transition delays could be achieved even if three-dimensional disturbances were included in the calculation. However, in all cases the delays were less than those predicted using a two-dimensional analysis. It is difficult to assess how good an approximation to the overall amplification is provided by the present calculations or the complete Cebeci-Stewartson analysis. This matter would be best resolved by considering an appropriately formulated initial value problem. In this case, the development of disturbances from a prescribed source, caused perhaps by a surface imperfection, would be calculated. However, the present

calculations do indicate that the three-dimensional disturbances are critically important in transition over compliant walls.

The calculations showed that anisotropic walls gave larger predicted transition delays than the isotropic walls. The use of an orthotropic plate in the isotropic wall case improved the local performance of the coating but did not change the predicted transition by a significant factor. It was shown that different transition delay characteristics could be obtained by optimizing the wall properties at different Reynolds numbers. This suggests that additional transition delays could be achieved by changing the wall properties in the axial direction. This has been examined recently by Carpenter[31] for two isotropic panels in series.

Finally, it was noted that oblique traveling-wave flutter instabilities have been found to remain marginally stable for all walls studied. So, as with the previous two-dimensional investigations, the Tollmien-Schlichting instabilities dominate transition.

The present analysis has considered three-dimensional primary instabilities. Further investigations are under way with these coatings. This includes wall property optimization for three-dimensional waves and the effect of wall compliance on secondary instabilities, Joslin and Morris.[32]

Acknowledgments

Support for this project for R. D. Joslin and P. J. Morris was supplied by the Naval Sea Systems Command and the Applied Research Laboratory Exploratory and Foundational Research Program under NAVSEA N00039-88-C-0051. Contributions by P. W. Carpenter were made while on study leave at the Department of Aerospace Engineering, The Pennsylvania State University. He would like to express his gratitude to that institution as well as the Office of Naval Research for their support. His work on compliant walls forms part of a longstanding research program at Exeter University supported by the Ministry of Defense (Procurement Executive). Preliminary work leading to the present paper was begun during a visit by P. J. Morris to Exeter University where he was in receipt of a visiting research fellowship provided by the Science and Engineering Research Council, United Kingdom.

References

[1]Kramer, M. O., "Boundary Layer Stabilization by Distributed Damping," *Journal of the Aeronautical Sciences*, Vol. 24, No. 6, 1957, pp. 459–460.

[2]Kramer, M. O., "Boundary Layer Stabilization by Distributed Damping," *Journal of the American Society of Naval Engineers*, Reader's Forum, 1960, p. 69.

[3]Kramer, M. O., "Boundary Layer Stabilization by Distributed Damping," *Journal of the American Society of Naval Engineers*, Vol. 72, No. 1, 1960, pp. 25–33.

[4]Kramer, M. O., "The Dolphins' Secret," *The New Scientist*, Vol. 7, 1960, pp. 1118–1120.

[5]Kramer, M. O., "Hydrodynamics of the Dolphin," *Advances in Hydroscience*, Vol. 2, 1965, pp. 111–130.

[6]Benjamin, T. B., "Effects of a Flexible Boundary on Hydrodynamic Stability," *Journal of Fluid Mechanics*, Vol. 9, Dec. 1960, pp. 513–532.

[7]Benjamin, T. B., "The Three Fold Classification of Unstable Disturbances in Flexible Surfaces Bounding Inviscid Flows," *Journal of Fluid Mechanics*, Vol. 16, July 1963, pp. 436–450.

[8]Benjamin, T. B., "Fluid Flow with Flexible Boundaries," *Proceedings in the 11th International Congress of Applied Mechanics*, Munich, 1964, Springer-Verlag, Berlin, pp. 109–128.

[9]Landahl, M. T., "On the Stability of a Laminar Incompressible Boundary Layer Over a Flexible Surface," *Journal of Fluid Mechanics*, Vol. 13, Aug. 1962, pp. 609–632.

[10]Gyorgyfalvy, D., "Possibilities of Drag Reduction by the Use of Flexible Skins," *Journal of Aircraft*, Vol. 4, No. 3, 1967, pp. 186–192.

[11]Daniel, A. P., Gaster, M., and Willis, G. J. K., "Boundary Layer Stability on Compliant Surfaces," British Maritime Technology Ltd., U.K. Internal Report, London, April 1987.

[12]Willis, G. J. K., "Hydrodynamic Stability of Boundary Layers Over Compliant Surfaces," Ph.D. Thesis, University of Exeter, Exeter, England, U.K., 1986.

[13]Gaster, M., "Is the Dolphin a Red Herring?," *Proceedings of the IUTAM Symposium on Turbulence Management and Relaminarisation*, edited by H. W. Liepmann and R. Narasimha, Springer-Verlag, New York, 1988, pp. 285–304.

[14]Carpenter, P. W., and Garrad, A. D., "The Hydrodynamic Stability of Flow Over Kramer-Type Compliant Surfaces: Part 1. Tollmien-Schlichting Instabilities," *Journal of Fluid Mechanics*, Vol. 155, June 1985, pp. 465–510.

[15]Carpenter, P. W., and Garrad, A. D., "The Hydrodynamic Stability of Flow Over Kramer-Type Compliant Surfaces: Part 2. Flow-Induced Surface Instabilities," *Journal of Fluid Mechanics*, Vol. 170, Sept. 1986, pp. 199–232.

[16]Carpenter, P. W., "Status of Transition Delay Using Compliant Walls," *Viscous Drag Reduction*, edited by D. M. Bushnell and J. N. Hefner, AIAA, Washington, DC, 1990, pp. 79–113.

[17]Riley, J. J., Gad-el-Hak, M., and Metcalfe, R. W., "Compliant Coatings," *Annual Review of Fluid Mechanics*, Vol. 20, 1988, pp. 393–420.

[18]Yeo, K. S., "The Stability of Flow Over Flexible Surfaces," Ph.D. Thesis, University of Cambridge, Cambridge, England, U.K., 1986.

[19]Carpenter, P. W., and Morris, P. J., "The Effects of Anisotropic Wall Compliance on Boundary Layer Stability and Transition," *Journal of Fluid Mechanics*, Vol. 218, Sept. 1990, pp. 171–223.

[20]Carpenter, P. W., and Morris, P. J., "Growth of Three-Dimensional Instabilities in Flow Over Compliant Walls," *Proceedings of the 4th Asian Congress of Fluid Mechanics*, Hong Kong, Aug. 1989, pp. I1–I3.

[21]Carpenter, P. W., and Morris, P. J., "The Hydrodynamic Stability of Flows Over Non-Isotropic Compliant Surfaces—Numerical Solution of the Differential Eigenvalue Problem," *Numerical Methods in Laminar and Turbulent Flow*, edited by C. Taylor, M. D. Olson, P. M. Gresho, and W. G. Habashi, 1985, Pineridge, Swansea, UK, pp. 1613–1620.

[22]Smith, A. M. O., and Gamberoni, H., "Transition, Pressure Gradient and Stability Theory," Douglas Aircraft Co., Long Beach, CA, Rept. ES26388, March 1956.

[23]Grosskreutz, R., "Wechselwirkungen zwischen turbulenten Grenzschichten und weichen Wänden," MPI für Strömungsforschung und der AVA, Göttingen, Germany, Mitt. No. 53, 1971.

[24]Grosskreutz, R., "An Attempt to Control Boundary Layer Turbulence with Non-Isotropic Compliant Walls," *University Science Journal Dar es Salaam*, Vol. 1, No. 1, 1975, pp. 65–73.

[25]Joslin, R. D., and Morris, P. J., "The Sensitivity of Flow and Surface Instabilities to Changes in Compliant Wall Properties," *Journal of Fluid and Structures*, Vol. 3, No. 4, 1989, pp. 423–437.

[26]Nayfeh, A. H., "Stability of Three-Dimensional Boundary Layers," *AIAA Journal*, Vol. 18, No. 4, 1980, pp. 406–416.

[27]Cebeci, T., and Stewartson, K., "On Stability and Transition in Three-Dimensional Flows," *AIAA Journal*, Vol. 18, No. 4, 1980, pp. 398–495.

[28]Corke, T. C., and Mangano, R. A., "Resonant Growth of Three-Dimensional Modes in Transitioning Blasius Boundary Layers," *Journal of Fluid Mechanics*, Vol. 209, Dec. 1989, pp. 93–150.

[29]Carpenter, P. W., and Gajjar, J. S. B., "A General Theory of Two- and Three-Dimensional Wall-Mode Instabilities in Boundary Layers Over Isotropic and Anisotropic Compliant Walls," *Theoretical and Computational Fluid Dynamics*, Vol. 1, No. 6, 1990, pp. 349–378.

[30]Carpenter, P. W., "A Note on the Hydroelastic Instability of Orthotropic Panels," *Journal of Sound and Vibration*, Vol. 94, No. 4, 1984, pp. 553–554.

[31]Carpenter, P. W., "Optimization of Multi-Panel Compliant Walls for Transition Delay," *Bulletin of the American Physical Society*, Vol. 35, No. 10, 1990, p. 2291.

[32]Joslin, R. D., and Morris, P. J., "The Effects of Compliant Walls on Secondary Instabilities in Boundary Layer Transition," AIAA Paper 91-0738, Jan. 1990.